Combined Microindentation and Synchrotron Radiation Microdiffraction Applied to Polymers

A. Gourrier, M. C. García Gutiérrez, and C. Riekel*

European Synchrotron Radiation Facility, B.P. 220, F-38043 Grenoble Cedex France

Received May 1, 2002; Revised Manuscript Received July 12, 2002

ABSTRACT: A Vickers microindentation setup has been developed for in situ X-ray microdiffraction with synchrotron radiation at the ESRF microfocus beamline (ID13). Ex situ experiments performed on a Nylon 66 fiber show changes in chain orientation in the indented zone, but the crystallinity remains unchanged. Similar experiments for an UHMW−PE fiber show a breakup of the orthorhombic phase into domains due to plastic deformation and a partial transformation of the orthorhombic phase into the monoclinic phase. In situ experiments during indentation of an UHMW−PE fiber show domain doubling during indentation and single domain recovery after the tip has been retracted.

Introduction

Microindentation is one of the simplest methods for determining the microhardness of materials including polymers.[1,2] Although it is in many cases possible to correlate the microhardness of a polymeric material with its microstructure,[3] structural changes occurring during indentation are not accessible directly unless the vicinity of the indenter tip is probed. Ideally, this should occur during indentation. A limited amount of such experiments have been reported, and selected examples will be mentioned.

Scanning electron microscopy (SEM) has been used to study the push-out of fibers in composite materials.[4] This technique is sensitive to changes in geometry and topography but does not provide atomic resolution data. Atomic force microscopy (AFM) has been applied to polymer surfaces but is not bulk sensitive.[5] In situ microspectroscopy during microindentation on semiconductors[6] provides local information on a molecular scale and could also be applied to polymers. Transmission electron microscopy (TEM) provides structural resolution in hard materials during nanoindentation.[7] Experiments on polymers would, however, be difficult due to the necessity of making ultrathin sections and radiation damage problems. X-ray diffraction experiments on bulk changes in the vicinity of an indenter tip have, however, to our knowledge not been reported.

The aim of the present article is to demonstrate the feasibility of such experiments for a synchrotron radiation (SR) microbeam of a few micrometers in diameter. A Vickers-type microindenter was used in view of the highly symmetric stress field around the tip, which simplifies data analysis, and the commercially available technology. In addition, an extensive literature on the application of Vickers microindentation to polymers is available.[3]

Experimental Section

Indentation Setup. The setup is shown schematically in Figure 1. together with an image of the sample environment. The sample stage consists of a motorized *x*/*y*/*z* gantry (MICOS), which allows displacing the sample with micrometer-precision. The stepping motors are interfaced to the ESRF VME control system.

Samples are glued to the edge of the flat surface of a diamond crystal so that the indented part is free from constraints during deformation. For this geometry, X-ray absorption effects of the support structure can be neglected. A motorized turret (OLYMPUS) allows switching between the indenter head with Vickers-type square-based diamond pyramid (MHT-10: PAAR) and two microscope objectives. A color CCD camera is attached to the setup, which allows collecting and digitizing the image via a PC-based video-card (MATROX). Forces applied on the indenter tip can be chosen within a range of 5 mN to 4 N and defined along with loading rate and dwell time through an external control box, which is interfaced to a PC. Forces were applied normal to the beam direction.

Materials. Experiments reported below were performed on fibers, which has advantages in view of the highly symmetric fiber geometry. For quantitative microhardness testing correction factors are needed,[2] but were not used in this study.

Nylon 66 was examined as an example of a semicrystalline fiber (about 50% amorphous phase) and UHMW−PE as an example for a fiber with a low amorphous content. High tenacity Nylon 66 filaments were obtained from Goodfellow Cambridge Ltd. Single fibers of 19 μm average diameter were separated by tweezers under a microscope. UHMW−PE filaments, composed of 12 μm average diameter fibers, were also obtained from Goodfellow Cambridge Ltd. More details on the UHMW−PE fiber have been reported elsewhere.[8] Single fibers were cut in length by microscissors and glued to the support as described above.

Synchrotron Radiation Experiments. SR-experiments were performed at the microfocus (ID13) beamline of the European Synchrotron Radiation Facility (ESRF).[9] A 5 μm monochromatic beam of wavelength $\lambda = 0.097_6$ nm was generated by the combination of focusing mirror and collimator. A slow-scan 16 bit-readout CCD detector (*X-ray Associates*; XRA) with a 130 mm diameter X-ray converter screen was used for routine data collection. Readout time was about 4 s/frame (single image in a sequence). For faster processes, a 12 bit-readout Gemstar detector (PHOTONIC) was used. Frames of 0.5 s were recorded while the readout time to disk was about 1.5 s. Control of the microindenter, detectors and the *x*/*y*/*z* gantry was possible with the ESRF SPEC interface.[10] The sample-to detector distance and the center of the detector were calibrated by an Ag−behenate standard.[11] Data were reduced and analyzed using the FIT2D software package.[12]

Calibration. The setup was calibrated by a GaN microcrystal glued to a glass fiber tip, which shows luminescence in the visible range when excited by the X-ray beam. The position of the GaN microcrystal was matched to the X-ray beam position and the focal point of the microscope. An additional calibration of the indenter tip was achieved by replacing the microcrystal with a thin Kapton-foil on the diamond support. The foil was then indented and the distance

* Corresponding author.

10.1021/ma0206725 CCC: $22.00
Published on Web 09/11/2002

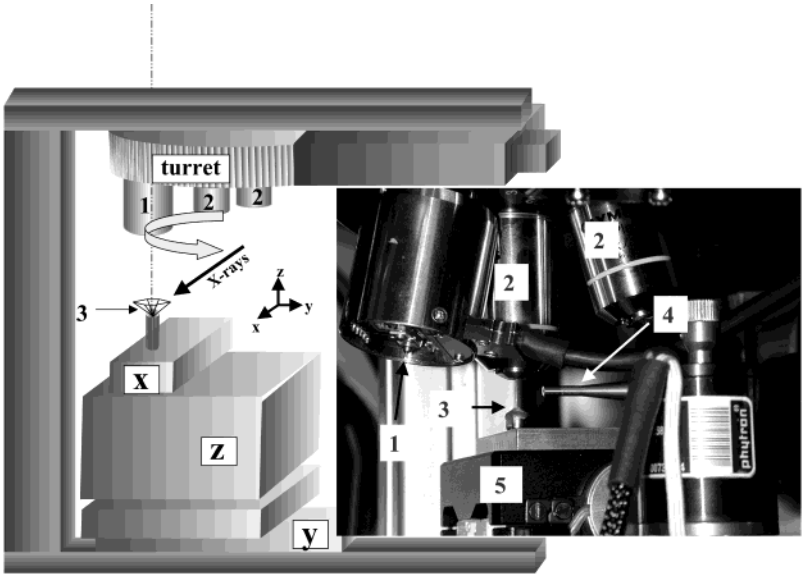

Figure 1. Schematic design of indenter setup. The direction of the X-ray beam is along the *x*-direction. The force is applied along the *z*-direction. The direction of movements of the *x*/*y*/*z* gantry is indicated: (1) indenter, (2) microscope objectives, and (3) diamond support. The inset shows a picture of the sample environment: (1) Vickers-type diamond tip, (2) microscope objectives, (3) diamond support, (4) microcollimator, and (5) *x*/*y*/*z* gantry.

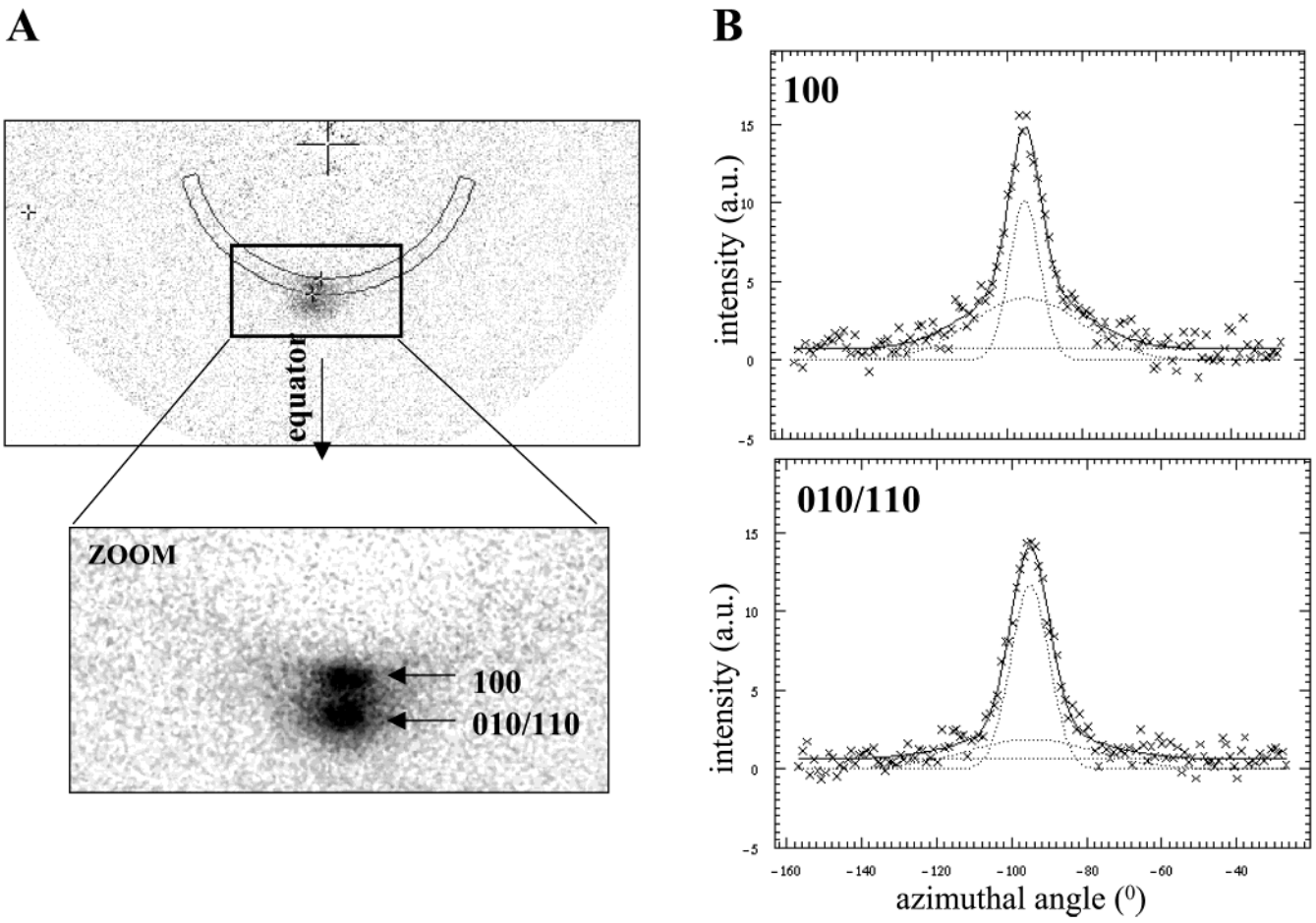

Figure 2. (A) Diffraction pattern of a Nylon 66 single fiber omitting the top part, which is partially shadowed by the indenter head. (B) Radial cake integration performed in the zone indicated in order to obtain the azimuthal profile of the 100 reflection. The corresponding fit for the 010/110 reflections is shown below. The profile was fitted by two Gaussian functions and a first-order polynomial background.

of the focal point from the center of the indentation determined. A sample could then be positioned laterally and vertically in the beam with a precision of about ± 1 μm. It was thus possible to reproducibly position fibers in the beam with diameters down to about 10 μm.

Results and Discussions

Ex Situ Experiments. A. Nylon 66. Figure 2a shows part of a Nylon 66 pattern from a single fiber. Indices are based on the triclinic α-phase.[16] The upper

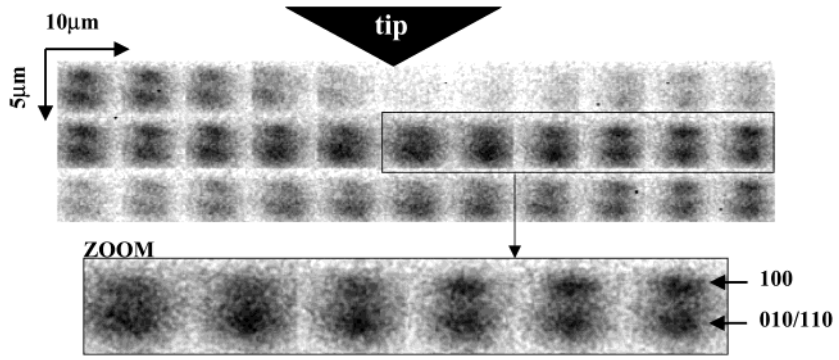

Figure 3. Composite image of the indented zone limited to the 100, 010/110 reflections. Mesh increments are $10_{\text{horizontally}} \times 5_{\text{vertically}}$ μm.

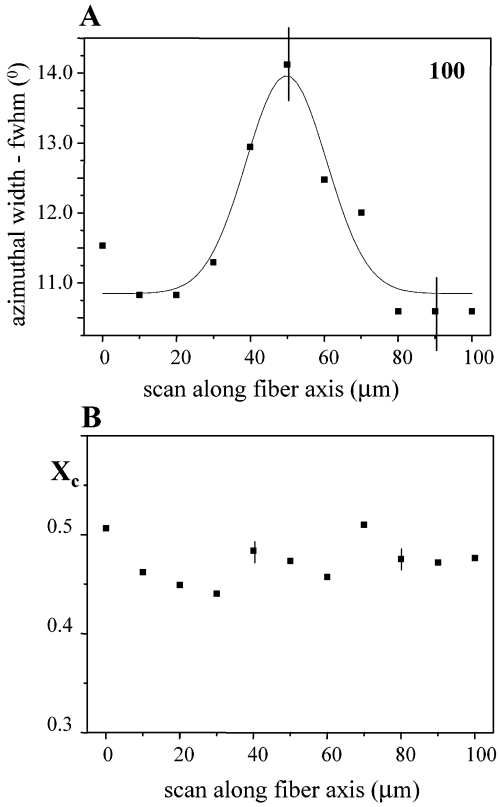

Figure 4. (A) Variation of azimuthal width (fwhm; degrees) of the 100 reflection across indented zone. A Gaussian function was fitted to the values. (B) Variation of crystallinity across the indented zone (error bars correspond to σ values).

part of the image was partially shadowed by the indenter head and is not shown. The intensity was integrated in radial direction within the segment of an annulus in order to determine the azimuthal intensity profile of the two peaks corresponding to the 100 and 010/110 reflections (Figure 2b). The peak profiles were fitted by two 1D-Gaussian functions corresponding to a Bragg peak and an amorphous halo. The background was fitted by a first-order polynomial.[17] The amorphous halo appears to be more prominent for the 100 reflection than for the 010/110 reflections. For further analysis of integral peak intensity, a radially larger segment was selected that allowed integrating both peaks and an amorphous halo.

The sample was indented with a 75 mN force (loading rate, 3 mN/s; hold, 10 s). Immediately afterward, the sample was mapped by scanning diffractometry (mesh: $10_{\text{horizontally}} \times 5_{\text{vertically}}$ μm). Measuring time per frame was 5 s. The composite image (Figure 3) is limited to the area of the 100 and 010/110 reflections.

The first row of frames shows in the middle a reduction of intensity due to the impression left by the indenter. The intensity distribution is also slightly asymmetric at the edges, which suggest that the fiber has slightly tilted after indentation. The second line shows no further trace of an intensity reduction but rather an increase toward the center. This is due to a geometric effect, as the indenter will slightly deform the fiber so that the thickness increases normal to the applied force. Scattering due to conformationally disordered chains (Brill transition[18]) was not observed.

It is of interest to analyze the second line in more detail and to determine whether the stress field induced by the indenter tip modified the chain orientation. The azimuthal width (full width at half-maximum; fwhm) and intensity of both reflections was found to increase at the point of indentation. This is shown in Figure 4a for the azimuthal width of the 100 reflection profile. It suggests a local perturbation of orientation distribution of crystalline blocks along the chain direction due to a plastic deformation. The fit of a Gaussian function to the variation of azimuthal width indicates that this static perturbation extends horizontally by about ± 20 μm (4σ). A systematic mapping of the perturbation across the indented zone should allow determining a projection of the stress distribution without the necessity of finite element calculations.[19]

The crystallinity (X_c) was determined from the sum of the Bragg intensities of the two equatorial peaks (ΣI_b) and the corresponding amorphous fraction (I_a) via

$$X_c = \Sigma I_b / \Sigma (I_b + I_a) \qquad (1)$$

X_c does not vary across the scanned zone (Figure 4b), which suggests that the orientation perturbation is not associated with a change in crystallinity.

B. Ultrahigh Molecular Weight Polyethylene. Figure 5a. shows the equatorial pattern of a single UHME−PE fiber recorded within 5 s with the beam at the center of the fiber using the slow scan CCD detector. The background scattering has been subtracted. The strongest reflections correspond to the orthorhombic PE phase. The presence of a weak fraction of monoclinic phase[14,15] has been observed previously by single fiber microdiffraction.[8] The fiber was indented with a 10 mN force (loading rate: 1 mN/s; hold: 10 s). The indented area was mapped by scanning diffractometry (mesh: $10_{\text{horizontally}} \times 5_{\text{vertically}}$ μm).

The composite image (Figure 5b) is limited to the area of the $110_0/200_0$ and 001_m reflections. The vertical size

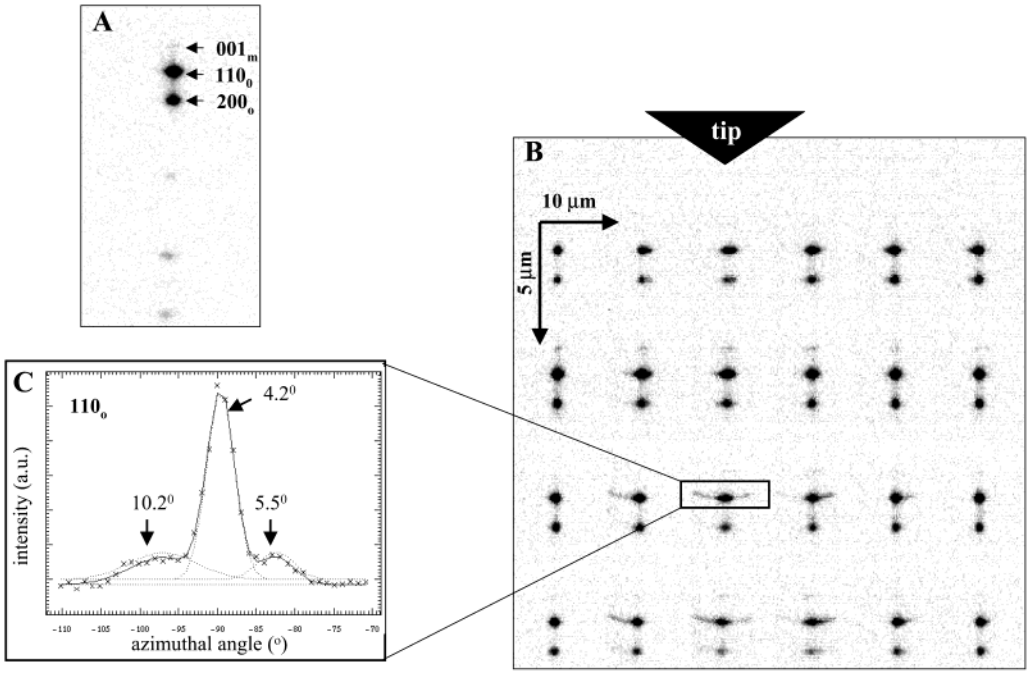

Figure 5. (A) Equatorial pattern of single UHMW−PE fiber. (B) Composite image of the indented zone in UHMW−PE limited to the $110_0/200_0$ and 001_m reflections. Mesh increments are $10_{\text{horizontally}} \times 5_{\text{vertically}}$ μm. (C) Azimuthal profile of a selected frame, which can be fitted by three Gaussian functions corresponding to a central domain and two satellite domains. The azimuthal width (fwhm) of the domains is indicated.

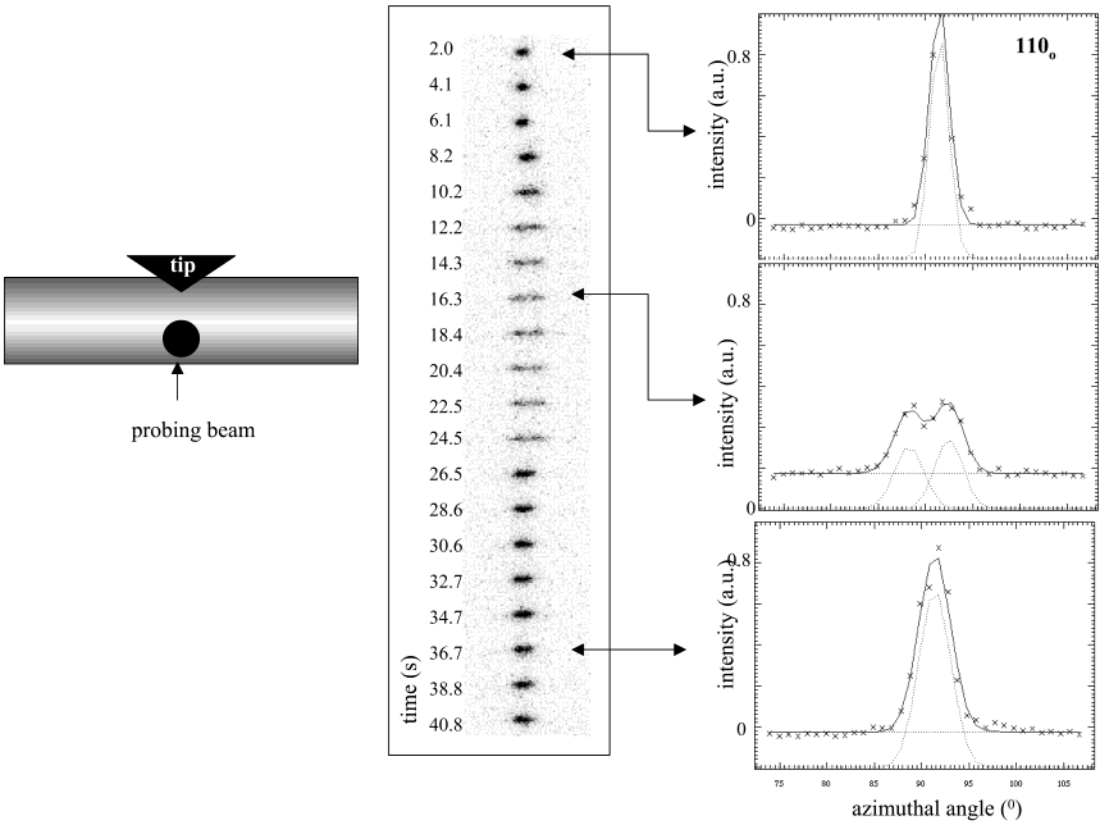

Figure 6. (A) Schematic design of in situ microindentation experiment. (B) evolution of 110_0 reflection during microindentation recorded by a fast-scan CCD detector. Selected azimuthal profiles of the 110_0 reflection are shown to the right. The profiles were fitted with one or two Gaussian functions (dotted lines). Solid lines correspond to the fitted profiles.

of the sample appears to be larger due to the convolution of beam diameter and sample diameter. The azimuthal width of the reflection in the top line increases at the indentation point as observed for Nylon 66 due to a local perturbation of crystalline block orientation distribution. The second line shows in addition the formation of the 100_m reflection of the monoclinic phase. It is known that the plastic deformation has to reach a critical value for monoclinic phase formation.[15] The third line shows that the azimuthal 110_0 reflection splits up into several domains. This suggests an irreversible plastic deformation that is beyond the elastic limit of the taut tie

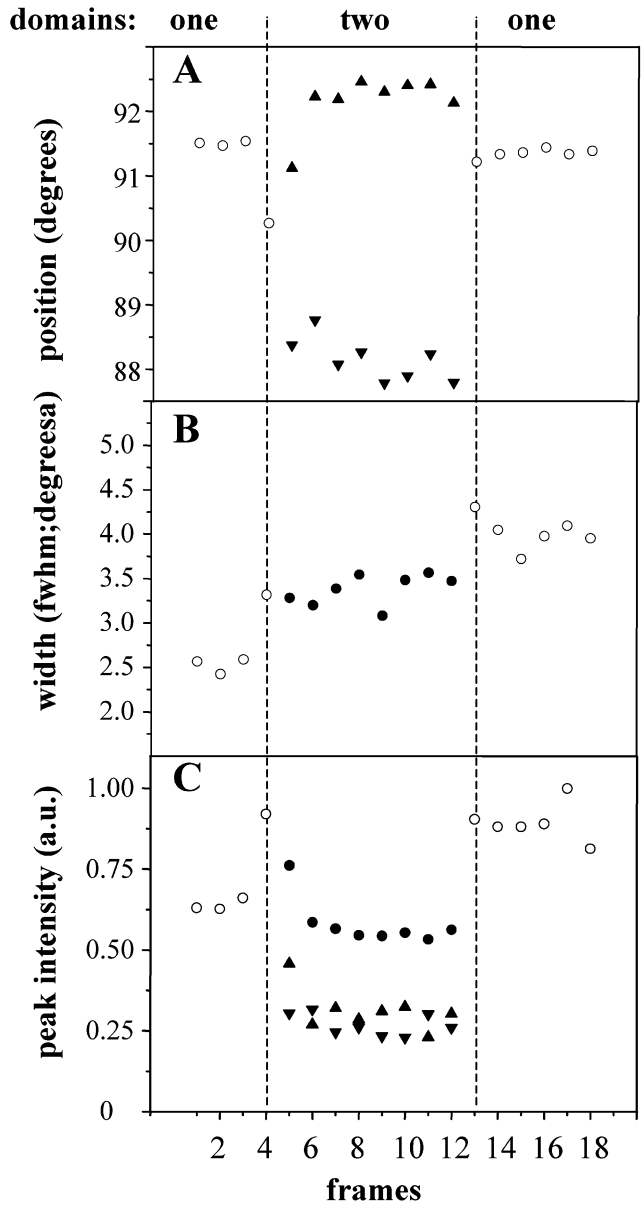

Figure 7. (A) Variation of 110_0 azimuthal peak position (degrees) during indentation. Open circles in the one-domain zone correspond to the fit of a single Gaussian function while triangles correspond to the fit of two Gaussian functions. (B) Variation of 110_0 azimuthal width (fwhm, degrees). Solid circles in the two-domain zone correspond to the average of the azimuthal width of the two Gaussian functions. (C) Variation of integral peak intensity (arbitrary units) of 110_0 reflection. Solid circles correspond to the sum of peak intensities (triangles).

molecules connecting the crystalline blocks (third line).[20] The position of the indenter tip can be easily recognized from the symmetry of the domain distribution. The satellite domains have a larger azimuthal width than the central domain as shown in Figure 5c.

The maximum of monoclinic phase formation seems to be just above the zone of irreversible domain formation, i.e., at a lower stress value. The domain formation obviously reduces the local stress required for monoclinic phase formation.

In Situ Experiments. To address time-dependent structural changes, an in situ experiment was performed on a UHMW−PE fiber with the probing beam below the center of the fiber (Figure 6.). The maximum force applied was 5 mN (loading rate, 1 mN/s; hold, 10 s).

The temporal variation of the 110_0 reflection profile shows a broadening of the azimuthal profile, which nearly returns to its original width after the tip has been retracted (Figure 6). Selected azimuthal profiles are shown to the right. The broadened profile can be fitted by two Gaussian functions. Prior to indentation and after retraction of the tip, a single Gaussian function can fit the profile. This suggests an elastic deformation where the taut tie molecules connecting the crystalline blocks are only elastically stressed as the crystalline blocks return nearly to their original orientation once the stress has been relieved. Static experiments on indented UHMW−PE will show only the end-state of this deformation.

A more detailed analysis of Gaussian profile parameters of the 110_0 reflection is shown in Figure 7. The variation of peak position (Figure 7a) shows that the one-domain zone is transformed during indentation into a two-domain zone. Retraction of the tip results again in a one-domain zone. The two-domain zone extends for about 15 s. In view of a loading rate of 1 mN/s and a 10 s hold time this implies that the probing beam "sees" the splitting up of domains nearly at the same time as the tip enters in contact with the fiber. Only the last frame in the one-domain zone is apparently influenced by the onset of deformation of the fiber. A shift in peak position and an increase in azimuthal width (Figure 7b) suggest that the chain orientation is perturbed locally by the stress field around the tip. The tip will expand the fiber normal to its trajectory, which will increase the scattering volume seen by the beam, and results in the intensity increase observed in frame 4. (Figure 7c) The azimuthal width remains constant in the two-domain zone and slightly increases further after retraction of the tip. (Figure 7b) This might be due to a remnant plastic deformation as already observed for Nylon 66 (Figure 4a). The integral peak intensity decreases again at the onset of the two-domain zone. (Figure 7c) In view of the small fiber diameter it is quite likely that the diamond tip will enter the outskirts of the probing beam which will reduce the scattering volume and can explain this intensity decrease. Upon retraction of the tip, the scattering volume will increase again and hence the intensity. The observation that the intensity remains at the same height as the last frame in the first one-domain zone (no. 4) suggests a remnant plastic deformation, which is also observed visually.

Conclusions

It has been shown that structural processes in polymers occurring in the vicinity of a Vickers indentation tip can be examined by X-ray microdiffraction. The use of diamond for the tip and the sample support allows absorption effects to largely be neglected. Faster readout time will allow exploring the splitting up of domains for UHMW−PE in more detail. In view of fiber diameters in the range of 10 μm, it will be necessary to apply in future experiments sub-μm beams that can be generated by various X-ray optical systems.[21−23] This will also allow bridging the gap to nanoindentation experiments. Small-angle X-ray scattering (SAXS) experiments should become possible down to a few μm beam size provided that a guard aperture can be introduced close to the sample.[24] The high heat conductivity of the diamond support will allow controlling the temperature of the sample.

Evidently other types of stress fields as generated by a Vickers-type tip are feasible. One should also note that this type of experiment is not limited to polymers.

Acknowledgment. The mechanical setup was developed with the help of J. Lange and L. Lardiere (ESRF). J. Meyer (ESRF) integrated the setup into the ESRF beamline control environment. M. Burghammer (ESRF) introduced the GaN alignment technique. T. Atkins (Bristol) provided structural parameters of Nylon 66. M.C.G.G. and C.R. wish to thank Prof. Baltá-Calleja (Madrid) for helpful discussions and suggestions. M.C.G.G. acknowledges as well the generous support of this investigation by a European Community Marie Curie Fellowship.

References and Notes

(1) Chandler, H., Ed. *Hardness Testing*, 2nd ed.; American Society of Metals: Metals Park, OH, 1999.
(2) Baltá-Calleja, F. J.; Martinez-Salazar, J.; Rueda, D. R. In *Encyclopedia of Polymer Science and Engineering*, 2nd ed.; Mark, H. F., Bikales, N., Overberger, C. G., Menges, G., Kroschwitz, J. I., Eds.; John Wiley&Sons: New York, 1987; Vol. 7.
(3) Baltá-Calleja, F. J.; Fakirov, S. *Microhardness of polymers*; Cambridge University Press: Cambridge, England, 2000.
(4) Janczak, J.; Buerki, G.; Rohr, L. *Key Eng. Mater.* **1997**, *127*−*131*, 623−630.
(5) Raghavan, D.; Gu, X.; Nguyen, T.; VanLandingham, M.; Karim, A. *Macromolecules* **2000**, *33*, 2573−2583.
(6) Gogotsi, Y.; Miletich, T.; Gardner, M.; Rosenberg, M. *Rev. Sci. Instrum.* **1999**, *70*, 4612−4617.
(7) Wall, M. A.; Dahmen, U. *Microsc. Res. Technol.* **1998**, *42*, 248−254.
(8) Riekel, C.; Cedola, A.; Heidelbach, F.; Wagner, K. *Macromolecules* **1997**, *30*, 1033−1037.
(9) Riekel, C. *Rep. Prog. Phys.* **2000**, *63*, 233−262.
(10) *Certified Scientific Software*; PO Box 390640 Cambridge, MA 02139.
(11) Blanton, T. N.; Huang, T. C.; Toraya, H.; Hubbard, C. R.; Robie, S. B.; Louer, D.; Goebel, H. E.; Will, G.; Gilles, R.; Raftery, T. *Powder Diffr.* **1995**, *10*, 91−95.
(12) Hammersley, A. P. *ESRF Internal Report*, ESRF97 HA02T, 1997.
(13) Tadokoro, H. *Structure of Crystalline Polymers*; Robert E. Krieger Publ. Comput. Inc.: Malabar, Florida, 1990.
(14) Turner-Jones, A. *J. Polym. Sci.* **1962**, *62*, S53−S56.
(15) Seto, T.; Hara, T.; Tanaka, K. *Jpn. J. Appl. Phys.* **1968**, *7*, 31−42.
(16) Bunn, C. W.; Garner, E. V. *Proc. R. Soc. London* **1947**, *189*, 39−68.
(17) Riekel, C.; Bränden, C.; Craig, C.; Ferrero, C.; Heidelbach, F.; Müller, M. *Int. J. Mol. Biol.* **1999**, *24*, 187−195.
(18) Xenopoulos, A.; Wunderlich, B. *Colloid Polym. Sci.* **1991**, *269*, 375−391.
(19) Rikards, R.; Flores, A.; Ania, F.; Kushnevski, V.; Baltá-Calleja, F. J. *Comput. Mater. Sci.* **1998**, *11*, 233−244.
(20) Penning, J. P.; Dijkstra, D. J.; Pennings, A. J. *J. Mater. Sci.* **1991**, *26*, 4721−4726.
(21) Bilderback, D. H.; Hoffman, S. A.; Thiel, D. J. *Science* **1994**, *263*, 201−203.
(22) Hignette, O.; Rostaing, G.; Cloetens, P.; Rommeveaux, A.; Ludwig, W.; Freund, A. In *SPIE Conference Proceedings 4499*; McNulty, I., Ed.; SPIE: San Diego, CA, 2001, pp 105−116.
(23) Müller, M.; Burghammer, M.; Flot, D.; Riekel, C.; Morawe, C.; Murphy, B.; Cedola, A. *J. Appl. Crystallogr.* **2000**, *33*, 1231−1240.
(24) Riekel, C.; Burghammer, M.; Müller, M. *J. Appl. Crystallogr.* **2000**, *33*, 421−423.

MA0206725